A megavoltage scatter correction technique for cone-beam CT images acquired during VMAT delivery

C. J. Boylan [1,2] , T. E. Marchant [1,2] , J. Stratford [3] , J. Malik [4] , A. Choudhury [4] , R. Shrimali [4] , J. Rodgers [3] , C. G. Rowbottom [1,2]

[1] Christie Medical Physics and Engineering (CMPE), The Christie NHS Foundation Trust, Wilmslow Road, Manchester M20 4BX, UK

[2] Manchester Academic Health Science Centre (MAHSC), Faculty of Medical and Human Sciences, University of Manchester, Manchester M13 9PL, UK

[3] Wade Centre for Radiotherapy Research, The Christie NHS Foundation Trust, Wilmslow Road, Manchester M20 4BX, UK

[4] Department of Radiation Oncology, The Christie NHS Foundation Trust, Wilmslow Road, Manchester M20 4BX, UK

Published in *Physics in Medicine and Biology* 57(12) pp. 3727 - 3740
http://iopscience.iop.org/0031-9155/57/12/3727

Abstract

Kilovoltage cone beam CT (kV CBCT) can be acquired during the delivery of volumetric modulated arc therapy (VMAT), in order to obtain an image of the patient during treatment. However, the quality of such CBCTs is degraded by megavoltage (MV) scatter from the treatment beam onto the imaging panel. The objective of this paper is to introduce a novel MV scatter correction method for simultaneous CBCT during VMAT, and to investigate its effectiveness when compared to other techniques. The correction requires the acquisition of a separate set of images taken during VMAT delivery, while the kV beam is off. These images – which contain only the MV scatter contribution on the imaging panel – are then used to correct the corresponding kV/MV projections. To test this method, CBCTs were taken of an image quality phantom during VMAT delivery and measurements of contrast to noise ratio were made. Additionally, the correction was applied to the datasets of three VMAT prostate patients, who also received simultaneous CBCTs. The clinical image quality was assessed using a validated scoring system, comparing standard CBCTs to the uncorrected simultaneous CBCTs and a variety of correction methods. Results show that the correction is able to recover some of the low and high contrast signal to noise ratio lost due to MV scatter. From the patient study, the corrected CBCT scored significantly higher than the uncorrected images in terms of the ability to identify the boundary between the prostate and surrounding soft tissue. In summary, a simple MV scatter correction method has been developed and, using both phantom and patient data, is shown to improve the image quality of simultaneous CBCTs taken during VMAT delivery.

1. Introduction

Volumetric modulated arc therapy (VMAT) is now established as an effective technique for delivering intensity modulated dose distributions comparable to fixed-beam IMRT (Yu and Tang, 2011). Crucially, VMAT offers a significant delivery time advantage due to the simultaneous rotation of the linear accelerator gantry, movement of the multi-leaf collimators (MLCs) and modulation of the dose rate (Otto, 2008; Cao *et al.*, 2009; Zhang *et al.*, 2010). The rotational geometry of VMAT delivery has more recently been exploited to acquire kilovoltage cone-beam computed tomography (kV CBCT) images concurrently during treatment, with the linac delivering the megavoltage (MV) treatment beam and a kV imaging beam orthogonally (Nakagawa *et al.*, 2009a; Nakagawa *et al.*, 2011).

There are a number of advantages in acquiring kV cone-beam images during treatment delivery. With the aim of treatment to deliver radiation doses safely but effectively, there is the increasing use of image-guided radiotherapy (IGRT) to ensure that the therapeutic ratio is optimized (Verellen *et al.*, 2008). Simultaneous cone beam imaging during VMAT allows IGRT to be performed with images of patient anatomy *in-vivo* rather than before or after treatment. Studies investigating intrafractional changes in patient position suggest there is an advantage to be gained from knowledge of internal anatomy during treatment (Nakagawa *et al.*, 2009b). Such knowledge could influence the choice of treatment margins and/or prescription dose, particularly for stereotactic patients, for whom accurate positioning is paramount (Sonke *et al.*, 2009). Simultaneous cone-beam imaging during VMAT also reduces the amount of in-room time for the patient, providing an advantage for department throughput.

While simultaneous cone-beam imaging is desirable, its quality is significantly degraded by MV x-ray scatter from the linac head, patient and support structures onto the kV imager (Williams *et al.*, 2004). The effect of this scatter is to introduce significant noise into the images, reducing the visibility of low contrast soft tissue boundaries and therefore making it difficult to perform soft tissue registration. Furthermore, any potential adaptive replanning strategy using simultaneous CBCTs is likely to be complicated by the difficulty in reliably outlining the target volume and organs at risk.

A number of solutions have been proposed to recover image quality, either by predicting the MV scatter contribution from the plan (Hugo *et al.*, 2008), through direct measurement of the scatter concurrently during delivery (van Herk *et al.*, 2011), or by avoiding MV scatter altogether by dividing the treatment arc into interlaced sectors for treatment and imaging (Ling *et al.*, 2011). Each of these methods have potential limitations. Prediction of the scatter using the treatment plan requires detailed knowledge of the linac motion and assumes that the scatter is uniform in the plane of the detector. The method proposed by van Herk *et al* (2011) notes that measurement of the scatter using alternate kV-on and kV-off frames halves the total number of projections for reconstruction, which may not cause major problems for slow treatments (i.e. stereotactic), but will reduce the quality of images taken during shorter delivery times. Furthermore, periodic interruption of the treatment beam for imaging, as described by Ling *et al* (2011), is appropriate only if plan quality is retained and delivery duration is not significantly increased. A direct measurement of MV scatter, which does not reduce the number of imaging frames or require the interruption of the treatment arc, is therefore desirable.

The purpose of this paper is to investigate the effectiveness of a novel MV scatter correction technique. In contrast to other proposed methods, the correction utilises a direct measurement of MV scatter such that it is patient and plan specific. Different variants of this method were first assessed through quantitative measurements of image quality on a phantom. The correction was then applied to three sets of simultaneous CBCT images from VMAT prostate treatments. A comparison of clinical image quality was then made, using an objective, validated scoring system for prostate CBCT images.

2. Method

2.1. Phantom Study

The image quality phantom used was the CATPhan 600 (Phantom Laboratory, Salem, USA), which was surrounded by additional scatter material to mimic the size and shape of the pelvis (Figure 1a). The phantom was set up at the isocentre of an Elekta

linear accelerator fitted with the Synergy CBCT system version 4.2 (Elekta, Crawley, UK). Reference cone beam images were taken (without MV delivery), using the standard prostate imaging protocol from this centre (parameters in Table 1).

CBCT acquisitions were then taken concurrently during three different VMAT deliveries. The deliveries were all previously treated VMAT prostate plans, typical of the current treatments at this centre, where the prescription is 57 Gy in 19# to the mean of the prostate. The plans were created using Pinnacle v.9.0 (Philips Medical Systems, Madison, USA) and consisted of a single 8MV arc, 4 degree control point spacing and a mean of 488 monitor units. In order to perform the scatter correction, the individual frames of the acquisition were retrieved for processing prior to back projection.

2.2. Scatter Correction Methodology

a) 2D scatter map from patient during treatment

A direct measurement of the scatter contribution was made by allowing the kV imager to acquire frames during VMAT treatment, but without a kV imaging beam. These scatter images are a series of 1024 x 1024 acquisitions taken at a constant frame rate over the treatment. The signal from these images is due only to the MV scatter received by panel, and therefore fluctuates over the course of the VMAT arc. For the CATPhan, the scatter images were taken immediately after the corresponding simultaneous MV/kV acquisition. As described later, the patient scatter images were acquired on a non-imaging treatment fraction.

Both the simultaneous CBCT frames, and the scatter images contain interference artefacts from the pulsing of the treatment beam, in the form of vertical lines. These artefacts were suppressed by identifying the position of the peaks and smoothing them. The scatter images also required further processing, such as the application of a ‘bad pixel’ mask and a median filter to remove excessive high frequency noise.

For all projections acquired using the Synergy system, the associated linac gantry angle is recorded. In order to carry out the scatter correction, software was written which cycled through the simultaneous CBCT images and found the closest scatter

image based on the gantry angle. A subtraction of the scatter image was then made. Details are given below of the other variants investigated for this study, and are shown schematically in Figure 2.

b) 1D uniform scatter map

The method described above uses a 2D image of the MV scatter for correction. However, it is apparent that there is no distinct structure or shape visible in the scatter images – instead they consist of a coarse 'glow' of higher signal intensity in the centre dropping slowly to the edges of the imager (Figure 3). Therefore, the scatter correction was also tested by subtracting the mean signal of each scatter image from the corresponding simultaneous image.

c) 2D scatter map from different scattering material

Methods (a) and (b) both utilise the MV scatter-only images taken during the CATPhan 'treatments'. In order to investigate the sensitivity of the MV scatter to patient size and shape, scatter images were also acquired using a different phantom. Delivering the same plans to the RANDO phantom (Phantom Laboratory, Salem, USA), pictured in Figure 1b, the scatter images were acquired again and scatter correction was applied as described in (a) on the simultaneous CATPhan projections.

d) Analytical Correction

Hugo *et al* (2008) suggests that the MV scatter at a given gantry angle can be estimated with the product of the dose rate and the field size at that point. In order to compare this analytical model to direct measurement of scatter, each treatment plan was run through a VMAT delivery emulator (Boylan *et al.*, 2011) to predict the dose rate over the arc. The exposed field area was also calculated for each gantry angle. An estimate of MV scatter was made by multiplying these values and applying a single empirical scaling factor based on experiment. For each simultaneous MV/kV projection, the estimated scatter was then subtracted prior to reconstruction.

For methods (a)-(d), the corrected projections were reconstructed using the same algorithm as the standard prostate kV-only CBCTs. Using the CTP404 test module within the CATPhan, low and high contrast signal to noise ratios (SNR) were

measured for the standard CBCTs, the uncorrected simultaneous CBCTs, and the four scatter corrected CBCTs (a)-(d). The low contrast SNR was calculated as:

$$\mathrm{SNR}_{\mathrm{low}} = \frac{\bar{x}_{LDPE} - \bar{x}_{PMP}}{\sigma_{centre}}$$

Where $\bar{x}_{LDPE}$ is the mean signal in the LDPE (low-density polyethylene) insert, $\bar{x}_{PMP}$ is the mean signal in the PMP (polymethylpentene) insert, and σ_{centre} is the standard deviation of the signal in the centre of the CATPhan. The high contrast SNR was calculated similarly but using the signals from the Delrin® insert (which has a similar density to cortical bone) and PMP.

2.3. Patient Study

A study is ongoing in this centre investigating the clinical value of CBCT images acquired simultaneously with VMAT delivery. The Simultaneous Cone-beam during Arc Therapy (SCART) study is a non-randomized phase 1 trial in which standard VMAT prostate patients (57 Gy in 19#) receive four simultaneous CBCTs over the course of their treatment. The usual imaging protocol at this centre is to take a minimum of 6 CBCT during treatment, on fractions 1, 2, 3, 6, 11 and 16. In addition to this, the SCART patients receive simultaneous CBCTs on fractions 2, 6, 11 and 16. By comparing the simultaneous CBCTs to the standard CBCTs taken on the same fraction, the ultimate aim of the SCART study is to assess whether these images are appropriate for clinical decision-making – i.e. the ability to perform soft tissue registration to reliably assess the coverage of the target volume and avoidance of organs at risk.

For the present study, the 6th fraction images from the first 3 SCART patients were retrieved. For each patient, a standard CBCT (parameters as in Table 1) and a simultaneous CBCT were acquired on this fraction. The MV scatter images, required for correction, were acquired as described in section 2.2 during a non-imaging fraction of the patient's treatment. For example, the scatter images for patient 1 were taken during fraction 10 of 19.

Clinical image quality was assessed using a validated scoring system developed for the SCART trial, which is specific to prostate cone-beam imaging. The scoring system (shown in Table 2), consists of a five tiered scale where 1 is a high quality image in which the soft tissue boundary of the prostate is clearly visible, and 5 is a clinically inadequate CBCT with which IGRT cannot be reliably carried out.

For the three patients, the clinical image quality scores were compared between the standard CBCT, the uncorrected simultaneous CBCT, and the 2D scatter corrected images as described in (a). In addition, to determine the effectiveness of simplified scatter models, the uniform scatter corrected images (b) and the analytical (predicted) scatter corrected images (d) were also included. Therefore, 15 separate CBCTs were scored. Four observers (two clinicians and two treatment radiographers) assessed the anonymized CBCTs independently. The order of the CBCTs was randomised for each observer and 6 repeat images were inserted in order to monitor intra-observer consistency. The average score for each CBCT was then calculated and compared.

3. Results

3.1. Phantom Study

Figure 4a shows how the mean signal from each projection varies over the arc. In comparison to a standard CBCT, the simultaneous projections consist of large peaks corresponding to sectors of the arc in which MV scatter is the highest. The effect of the correction is to reduce the excess scatter signal from these frames. The spikes in the corrected projections are due to small angular mismatches between the scatter images and the simultaneous projections. The effect of these spikes was mitigated through the application of a median filter prior to CBCT reconstruction.

Figure 4b shows the mean MV scatter signal from each of the correction methods over a delivery arc. The ‘true’ scatter signal (solid line) was determined by subtracting the standard (kV-only) projections from the simultaneous (kV/MV) projections. The signal from methods (a) and (b) is due only to the MV scatter contribution with the CATPhan on the treatment couch and has a correlation coefficient of 0.91 when compared to the ‘true’ scatter signal. The signal from method (c), which has the RANDO phantom on the couch, offers an approximation of the CATPhan scatter, and

a correlation coefficient of 0.89. Method (d), which only uses the plan data, differs in magnitude from the other measurements, and has a correlation coefficient of 0.78.

The effect of the MV scatter reduces the low contrast SNR from 3.2 (standard CBCT) to 2.0 (simultaneous CBCT) and the high contrast SNR from 11.3 to 3.0. The four different scatter correction methods (a) – (d) improve the SNRs by different amounts, as shown in Figure 5. Method (a), employing the full 2D scatter images, shows the largest recovery of SNR. The analytical correction (d) showed the smallest increase in SNR compared to the uncorrected images.

3.2. Patient Study

The inter-observer variation for the scoring was low, with 19/21 CBCTs graded within 1 point of each other. Each of the four observers also viewed 6 repeated CBCTs to monitor consistency. One of these repeat observations differed (by 1 point) from the observer's original scoring, which was considered an acceptable level of intra-observer variation. The average scores are shown in Table 3, and an example of the reconstructed CBCTs are shown in Figure 6.

The score for the uncorrected CBCTs was significantly worse than for the kV-only CBCTs - an average increase of 1.4 points on the scoring scale ($p=0.01$). In all patients the corrected images (using methods (a), (b) and (d)) scored better than the uncorrected images. Comparing the effectiveness of each method, the 2D scatter correction (a) resulted in the largest improvement, improving the quality score on average by 0.67 compared to the uncorrected CBCT ($p=0.04$). The 1D (uniform) correction, on average, improved the score by 0.54 points, but without significance over 3 patients ($p=0.1$), and the analytical correction improved the average score by 0.5 points ($p=0.03$).

4. Discussion

Simultaneous cone beam imaging during VMAT is a potentially useful technique which could influence the quality and efficiency of IGRT. It is anticipated that the ongoing SCART study will answer questions about the clinical value of such images, allowing for a safe change in imaging protocol in the future. Initial experiences of the

acquisition and reconstruction of simultaneous images has been broadly positive at this centre, although the MV scatter remains a problem.

The effect of MV scatter is clear from both the phantom and patient studies. Low contrast SNR was significantly decreased for the uncorrected images, which is an important parameter when attempting to discriminate between soft tissue interfaces. These results were supported by the patient images – the average image quality score was reduced by 1.4 for the uncorrected CBCTs. The observers noted that some of these images were inappropriate for IGRT, due to problems identifying any soft tissue boundary in the prostate region.

Four correction techniques were compared for the phantom study. Methods (a) to (c) utilized scatter images acquired during a VMAT delivery, while (d) used an analytical model derived from the treatment plan. The 2D correction (a) outperforms the uniform correction method (b), implying that the shape of the MV scatter image (Figure 3) is important for correction. Furthermore, comparing methods (a) and (c), which used a different phantom, it is apparent that the MV scatter contribution is somewhat dependant on the patient geometry (this is discussed further below). The clinical image scoring results support the phantom results, with the full 2D correction outperforming the uniform correction and the analytical method.

Of the options assessed in this study, a full 2D correction using scatter images acquired from the patient provides the biggest increase in image quality. However, the practicality of when to acquire these projections may be problematic. For the patients considered in this study, undergoing a standard offline imaging protocol, a pre-treatment CBCT to verify set-up will still be required on the first fraction. In this case, the scatter projections could be taken on fraction 1, and then used to correct simultaneous CBCTs from fractions 2, 3, 6, 11 and 16. However, for other fractionation schemes (such as stereotactic treatments), some alternate method of acquiring the scatter images will be needed.

It was observed that method (c), utilising a different scattering phantom, was able to recover some of the low and high contrast SNR for the CATPhan images – although not as much as method (a), which used the CATPhan itself as the scattering volume.

Potentially, scatter images from a phantom could be taken prior to a patient's first fraction on the treatment machine, and then used to correct the subsequent patient CBCTs. Work is underway to establish whether delivery to a pre-treatment dosimetric verification phantom can provide viable scatter images. It should be noted that the results presented here do not show a strong dependency on patient geometry, which may be due to the fact that the CATPhan and RANDO phantoms are not significantly different in terms of size and shape. Further work will be required to determine whether method (c) is still effective if there is a large disparity between the patient and the phantom shape.

The scatter correction method described here differs from previously reported methods. The technique proposed by van Herk *et al* interlaces kV imaging frames with MV scatter acquisitions, such that the correction can – in principle - be performed 'on the fly'. This method has clear benefits in that it does not require the acquisition of a separate scatter acquisition. However, due to the halving of the number of kV projections, the authors note that soft tissue contrast may be compromised for fast VMAT treatments. As there is a trend towards shorter VMAT treatment durations for standard fractionation regimes, the reduction in the number of frames becomes less desirable (although, reconstruction algorithms have been proposed for sparse projections (Choi *et al.*, 2010)). Conversely, for stereotactic radiotherapy treatments, the method proposed by van Herk *et al* becomes more useful, as the number of frames is large enough to produce clinically acceptable reconstructions.

The technique proposed by Ling *et al* effectively removes the problem of MV scatter by dividing the VMAT arc into sectors for imaging and treatment. Signal to noise ratio is retained, as only the scatter-free projections are selected for reconstruction. The authors anticipate that further engineering efforts are required to co-ordinate the switching between MV and kV delivery before it can be implemented widely. However, the periodic interruption of the treatment beam leads to an increase in treatment time, which may be at odds with the trend towards shorter VMAT deliveries. It is also not clear what effect the interruption has on the plan or dosimetric quality. In comparison, the scatter correction presented in this study has no impact on

the treatment duration, and allows the imager to acquire the standard number of projections for an acceptable CBCT.

The use of the analytical model – method (d) – did not perform as well as the direct measurements of MV scatter, but Figure 5 and Table 3 indicate that this technique did recover some image quality. Such a model would be beneficial as there would be no requirement for measurements on the linac prior to patient treatment. However, Figure 4b indicates that the model may require some refinement to more accurately approximate the scatter signal. In particular, it will be of interest to determine whether geometric characteristics of the patient (e.g. effective thickness at each gantry angle) could be included to improve the analytical model.

This study has shown that the application of a novel scatter correction method leads to an improved low and high contrast SNR on phantom CBCTs. Through the scoring of patient CBCTs, the corrected images were also observed to be of higher clinical quality. The results also suggest that a patient-specific direct measurement of scatter, rather than an analytical model-based approach, is required to best recover image quality.

Acknowledgements

The authors would like to thank the Wade Centre for Radiotherapy Research for their assistance with the clinical aspects of this study. The lead author's work is partially funded by an Elekta research grant.

References

Boylan C J, Rowbottom C G and Mackay R I 2011 The use of a realistic VMAT delivery emulator to optimize dynamic machine parameters for improved treatment efficiency *Phys Med Biol* **56** 4119-33

Cao D, Afghan M K, Ye J, Chen F and Shepard D M 2009 A generalized inverse planning tool for volumetric-modulated arc therapy *Phys Med Biol* **54** 6725-38

Choi K, Wang J, Zhu L, Suh T S, Boyd S and Xing L 2010 Compressed sensing based cone-beam computed tomography reconstruction with a first-order method *Med Phys* **37** 5113-25

Hugo G, Matuszak M M, Campbell J and Yan D 2008 Cone beam CT acquisition during volumetric arc radiotherapy delivery: correction for induced artifacts *Med Phys* **35** 2892

Ling C, Zhang P, Etmektzoglou T, Star-Lack J, Sun M, Shapiro E and Hunt M 2011 Acquisition of MV-scatter-free kilovoltage CBCT images during RapidArc or VMAT *Radiother Oncol* **100** 145-9

Nakagawa K, Haga A, Shiraishi K, Yamashita H, Igaki H, Terahara A, Ohtomo K, Saegusa S, Shiraki T, Oritate T and Yoda K 2009a First clinical cone-beam CT imaging during volumetric modulated arc therapy *Radiother Oncol* **90** 422-3

Nakagawa K, Kida S, Haga A, Masutani Y, Yamashita H, Imae T, Tanaka K, Ohtomo K, Iwai Y and Yoda K 2011 Cone beam computed tomography data acquisition during VMAT delivery with subsequent respiratory phase sorting based on projection image cross-correlation *J Radiat Res (Tokyo)* **52** 112-3

Nakagawa K, Shiraishi K, Kida S, Haga A, Yamamoto K, Saegusa S, Terahara A, Itoh S, Ohtomo K and Yoda K 2009b First report on prostate displacements immediately before and after treatment relative to the position during VMAT delivery *Acta Oncol* **48** 1206-8

Otto K 2008 Volumetric modulated arc therapy: IMRT in a single gantry arc *Med Phys* **35** 310-7

Sonke J J, Rossi M, Wolthaus J, van Herk M, Damen E and Belderbos J 2009 Frameless stereotactic body radiotherapy for lung cancer using four-dimensional cone beam CT guidance *Int J Radiat Oncol Biol Phys* **74** 567-74

van Herk M, Ploeger L and Sonke J J 2011 A novel method for megavoltage scatter correction in cone-beam CT acquired concurrent with rotational irradiation *Radiother Oncol* **100** 365-9

Verellen D, De Ridder M and Storme G 2008 A (short) history of image-guided radiotherapy *Radiother Oncol* **86** 4-13

Williams P, Sykes J and Moore C 2004 The effects of radiation scatter from simultaneous MV irradiation on kV fluoroscopic and X-ray volume imaging with the Elekta Synergy system (Abstract) *Radiother Oncol* **73** S229-30

Yu C X and Tang G 2011 Intensity-modulated arc therapy: principles, technologies and clinical implementation *Phys Med Biol* **56** R31-54

Zhang P, Happersett L, Hunt M, Jackson A, Zelefsky M and Mageras G 2010 Volumetric modulated arc therapy: planning and evaluation for prostate cancer cases *Int J Radiat Oncol Biol Phys* **76** 1456-62

Table 1. Reference cone beam imaging protocol for prostate patients

Tube potential	120 kV
Nominal mAs per frame	40 mAs
Collimation	Medium field of view (MFOV)
Imaging dose	7.9 mGy
Pulse length	16 ms
Approx. number of frames	~650

Table 2. Prostate CBCT image quality scoring scale

Score	**Description**
1	Able to define all interfaces between the prostate and peri-prostatic tissues. Appropriate for clinical decision making.
2	Able to identify the soft tissue interface between the prostate and the anterior rectum, *and* the prostate and the posterior-superior bladder. Appropriate for clinical decision making.
3	Able to identify the soft tissue interface between the prostate and the anterior rectum only. Appropriate for clinical decision making.
4	Difficult to define the interface between the prostate and the rectum/bladder, however, able to identify anterior ractal wall and thus infer the position of the posterior prostate border. Appropriate for clinical decision making.
5	Low quality image. Prostate, rectum and bladder appear as a homogenous mass with soft tissue delineation planes difficult to visualise, or too many artefacts to be able to infer the position of the prostate. Inappropriate for clinical decision making.

Table 3. Averaged quality scores for the three sets of patient images.

	Patient 1	Patient 2	Patient 3
Standard CBCT	1.7	1.7	2.0
Uncorrected simultaneous CBCT	3.0	2.3	4.3
Method (a) corrected	2.3	2.3	3.3
Method (b) corrected	2.0	2.0	3.7
Method (d) corrected	2.5	2.0	3.7

Figure 1. a) The CATPhan image quality phantom for kV CBCT, within additional scatter material, b) the RANDO anatomical phantom (torso only).

a)

b)

Figure 2. Schematic showing the correction strategies employed for the phantom imaging study.

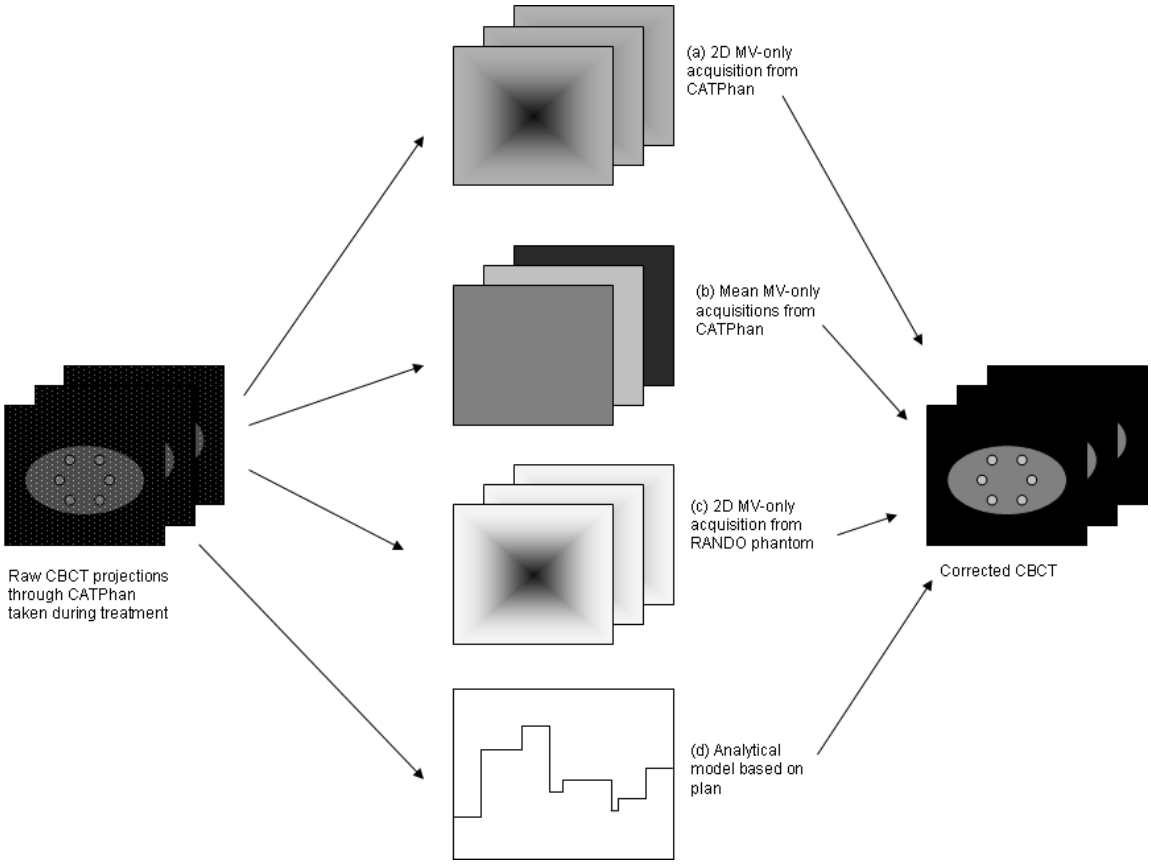

Figure 3. One of the MV scatter-only frames taken during VMAT delivery. Scatter correction method (a) utilises the full 2D data from these frames, whereas method (b) takes the mean signal.

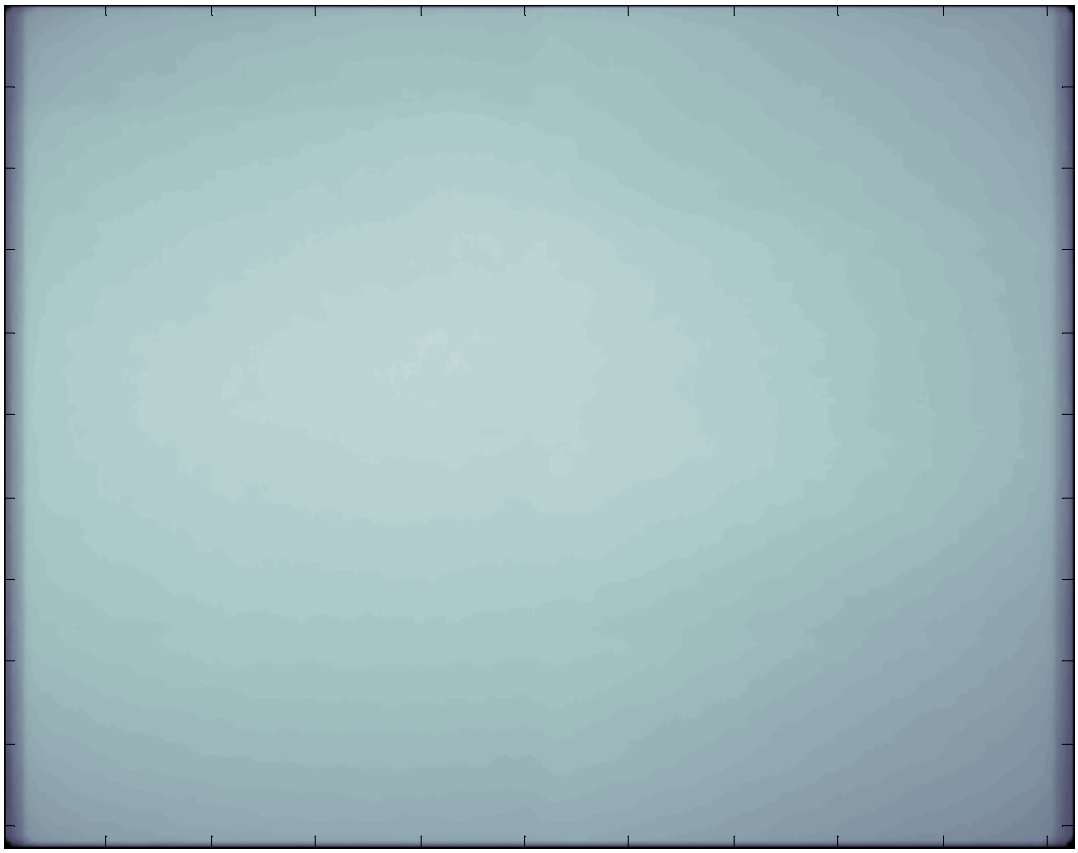

Figure 4. a) Mean image signal over a treatment arc for the CATPhan, b) comparison of the scatter signals over the treatment arc for each correction method

a)

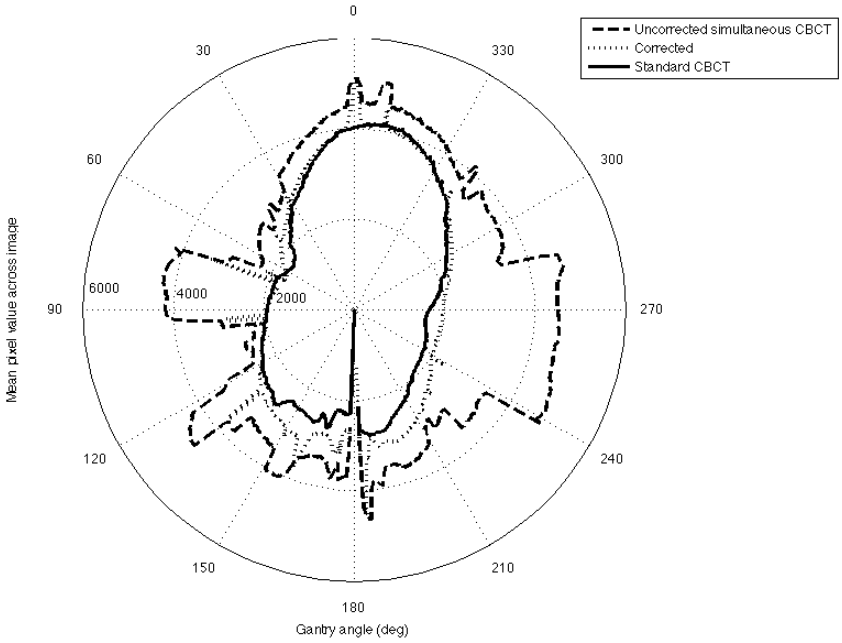

b)

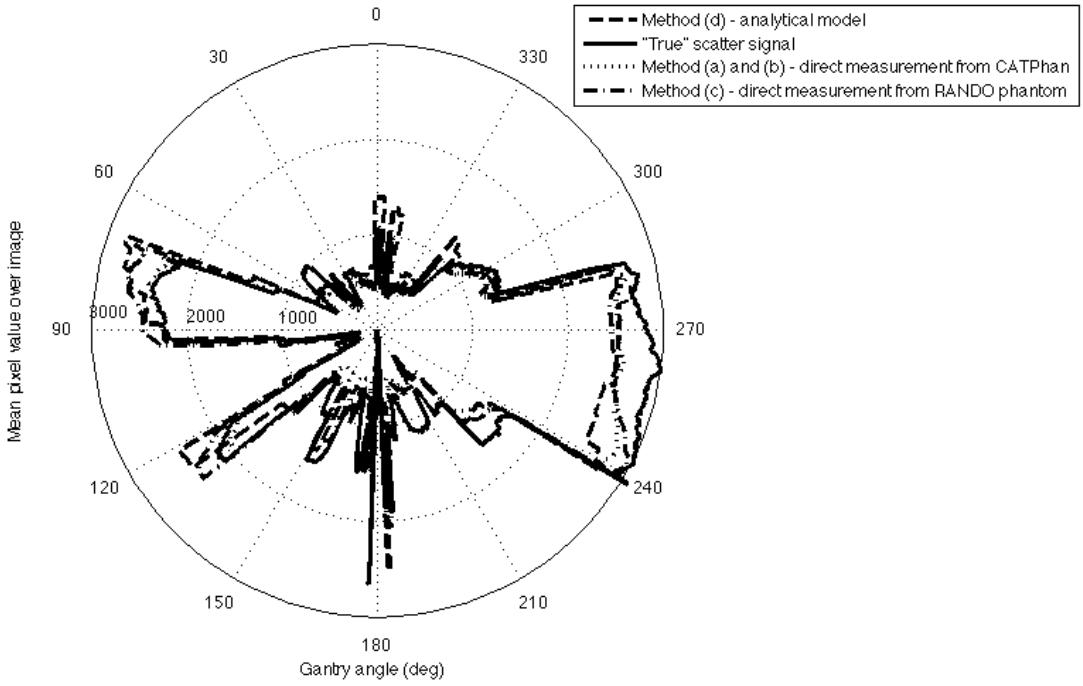

Figure 5. Comparison of low- and high-contrast SNR utilizing the different scatter correction techniques (a) – (d).

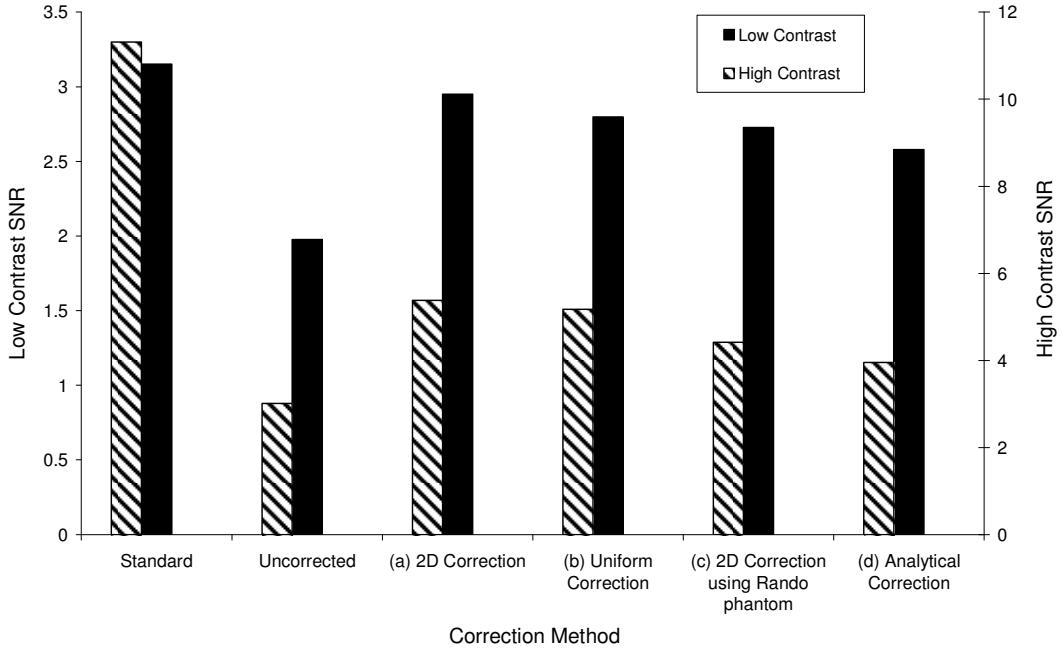

Figure 6. Single CBCT slice from patient 1. a) Standard CBCT taken prior to treatment, b) uncorrected CBCT taken during VMAT delivery, c) 2D correction (method a), d) uniform correction (method b), e) analytical correction (method d).

(a) 

(b) 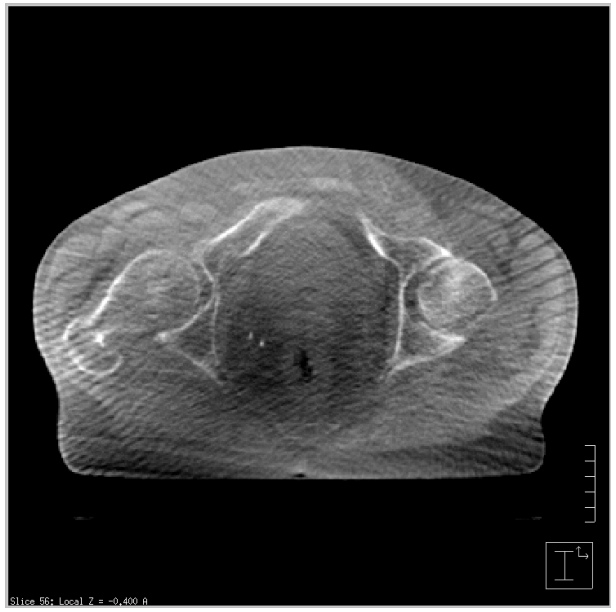

(c) 

(d) 

(e)